ACS Catalysis

Research Article

Cite This: ACS Catal. 2019, 9, 10940−10950

pubs.acs.org/acscatalysis

Unprecedented Copper(II) Complex with a Topoquinone-like Moiety as a Structural and Functional Mimic for Copper Amine Oxidase: Role of Copper(II) in the Genesis and Amine Oxidase Activity

Ritambhara Jangir, Mursaleem Ansari, Dhananjayan Kaleeswaran, Gopalan Rajaraman,*
Mallayan Palaniandavar,*,† and Ramaswamy Murugavel*

Department of Chemistry, Indian Institute of Technology Bombay, Powai, Mumbai 400076, India

Supporting Information

ABSTRACT: Copper amine oxidase (CAO), consisting of the topoquinone (TPQ) cofactor, catalyzes the oxidation of primary amines to aldehyde. We have successfully addressed this issue through isolation of a copper complex which mimics the active-site structure as well as the function of CAO. This inimitable complex, consisting of two TPQ-like side-arms, formed by ambient aerial oxidation of a precursor Schiff base complex, is the most efficient homogeneous catalyst for quantitative oxidation of primary benzylic amines to corresponding secondary imines under ambient conditions within 30 min. The longstanding contention of actual involvement of Cu(II) in the catalysis is resolved through quenching experiments of Cu(II) superoxo species and detailed density functional theory studies.

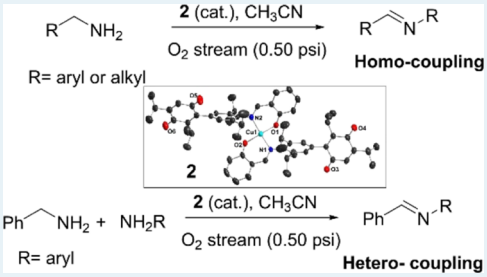

KEYWORDS: *copper amine oxidase, bioinspired catalysis, topoquinone, amine oxidation, mechanism*

INTRODUCTION

In nature, the oxidative transformation of amine to aldehyde is achieved by copper amine oxidase (CAO),[1] which is a quinoprotein containing Cu(II) and topoquinone (TPQ) cofactor in the active site (Figure 1a). This enzyme has inspired the development of several biomimetic homogeneous catalytic systems.[2] Many metalloenzyme-like catalytic systems which effect aerobic oxidation under very mild conditions, avoiding the use of copper metal, oxidants, and high temperatures, have been developed in the past.[3] For example, Wendlandt and Stahl developed an efficient biomimetic organo catalyst 4-*tert*-butyl-2-hydroxybenzoquinone (Figure 1b) for chemoselective aerobic oxidation of various benzylic amines to imines in the absence of copper or another redox catalyst at room temperature (RT).[3b] Eckert and Bruice reported that *o*-quinones acts as an efficient organocatalyst without requiring a metal for the chemoselective oxidation of benzylic amines.[3a] Yuan et al. devised a heterogeneous Pt/Ir bimetallic nanocluster with a 4-*tert*-butylcatechol redox-active organic cofactor for the aerobic oxidation of amines.[4] Largeron et al. have reported an environmentally friendly biomimetic method which involves a synergistic combination of copper and *o*-iminoquinone organocatalyst for the oxidation of primary aliphatic amines to imines, under ambient conditions.[5]

The biogenesis of TPQ in CAO proceeds via a self-processing mechanism and requires only O_2 and a Cu(II) in the active site, which are proposed to catalyze the hydroxylation of tyrosine to TPQ via (a) generation of dopamine, (b) hydration, and (c) oxidation.[6] This oxidation process is a two electron process aided by the redox metal as well as the cofactor, producing the aldehyde. Biochemical studies suggest that the Cu(II) active site required for the

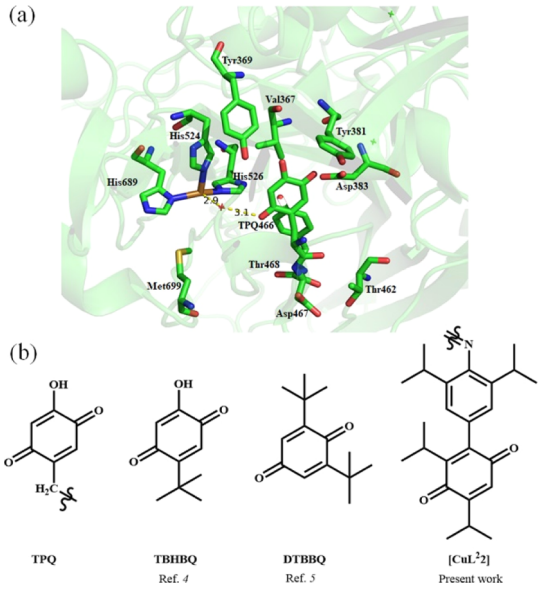

Figure 1. (a) Active site of *Escherichia coli* CAO; (b) TPQ and related models for amine oxidation.

Received: June 4, 2019
Revised: October 8, 2019
Published: October 17, 2019

DOI: 10.1021/acscatal.9b02326
ACS Catal. 2019, 9, 10940−10950

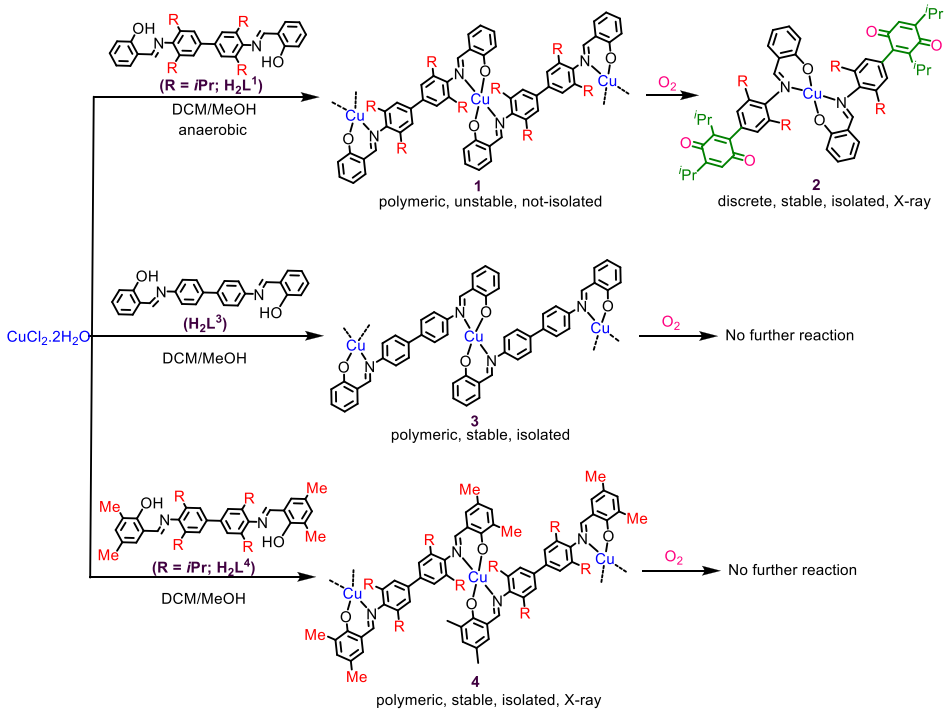

Figure 2. Synthesis of **2**, **3**, and **4**.

biosynthesis of the quinone cofactors is not involved in subsequent amine oxidation.[6b] Substituted 1,4-benzoquinone compounds are usually the products of oxidation of anilines, and their synthesis is determined by factors like basicity of the amino group, pH of the medium, and the aromatic substituents.[7] All these systems require extreme reaction conditions, tedious work-up, and so forth and often with low yields of the product.[7b]

Herein, we report facile synthesis of a novel Cu(II) complex containing two *p*-quinone moieties analogous to the TPQ cofactor of the CAO enzyme. Interestingly, this complex mimics the amine oxidase activity by converting primary amines to imines in a good yield at RT using dioxygen as the oxidant. The mechanisms for both the genesis of the *p*-benzoquinone moiety from the benzidine moiety and the catalytic oxidation of benzylic amines to imines have been proposed, illustrating the role of coordinated Cu(II) in both genesis and acceleration of amine oxidase activity.

RESULTS AND DISCUSSION

Synthesis and Characterization of $[Cu(L^2)_2]$ (2). The green solution obtained by mixing $CuCl_2{\cdot}2H_2O$ with the ligand (H_2L^1)[8] (1:2.5) in DCM/MeOH turns brown within a few minutes. This solution affords single crystals of $[Cu(L^2)_2]$ (**2**), with 60% yield, on standing for two weeks, rather than the anticipated $[CuL^1]_n$ (**1**) (Figures 2 and S1–S12). The IR spectral band at 1645 cm^{-1} is because of ν(C=O).[9] The electrospray ionization-mass spectrometry (ESI–MS) reveals the molecular ion peak at m/z 1003.39. The band appearing at 463 nm in the UV–vis spectrum of **2** is similar to n → π^* transition observed for *p*-quinone derivatives.[7b] The electronic absorption spectrum shows two intense ligand field features (920 and 816 nm) along with a low intensity shoulder, revealing strong axial perturbation of the CuN_2O_2 coordination plane by the solvent. The electron paramagnetic resonance (EPR) spectrum of **2** recorded in a mixture of CH_2Cl_2/toluene (1:4 v/v) yielded a fairly resolved spectrum revealing a larger g_z value compared to g_x and g_y, indicating the presence of unpaired electron in the $d_{x^2-y^2}$ orbital (Figures S8 and S9). This is consistent with the distorted square-based geometry and the density functional theory (DFT) calculations (see twist calculations in the Supporting Information).[10] In the molecular structure of **2**, the central Cu(II) is coordinated to two deprotonated HL^2 (Figure 3) with a significantly distorted

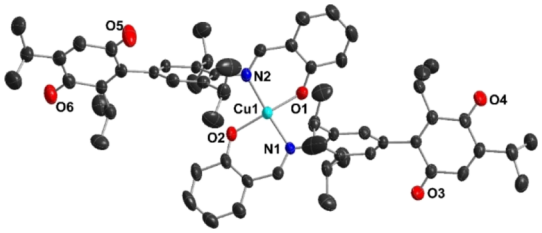

Figure 3. ORTEP (30% probability) drawing of **2**.

square planar geometry with trans bond angles of 152.66(15)° and 158.70(16)°. The C=O bond lengths (1.213(6)–1.225(6) Å) are comparable to those found in *p*-benzoquinones.[7b]

Possible Pathway for Formation of 2, the Role of O_2. When the reaction leading to **2** was repeated by strictly excluding oxygen, the initial green solution obtained remained stable even after 15 days without turning brown. The ESI–MS of this green solution exhibits a peak at m/z 661.41 corresponding to the $[CuL^1 + K]^+$ ion, the monomeric unit of **1**. The absorption spectrum of this oxygen degassed reaction mixture (presumably **1**) displays an intense band at 381 nm (Figure S11) and ligand field bands at 731, 815, and 918 nm (Figure S12), revealing the presence of a square-based Cu(II) coordination geometry. The frozen solution EPR spectrum

DOI: 10.1021/acscatal.9b02326
ACS Catal. 2019, 9, 10940–10950

(Figure S13) is axial ($g_{\|}$ 2.410; $A_{\|}$ 139 × 10^{-4} cm^{-1}), typical of the Cu(II) ion in a square planar geometry.

Interestingly, when $CuCl_2{\cdot}2H_2O$ is treated with $\mathbf{H_2L^3}$ or $\mathbf{H_2L^4}$, the initially formed polymeric complexes **3** or **4** (Figure S14) do not undergo further ligand oxidation as in the case of **1** (Figures 2 and S1). The difference in the reactivity of H_2L^1 in comparison to H_2L^3 or H_2L^4 can be understood based on the substituents present in the ligand system as depicted in Figure S15. While the presence of isopropyl substituents on the benzidine ring favors ligand scrambling in **D** (+I effect), the absence of methyl or any other substituents on the salicylic ring facilitates initial hydrolysis of the imine linkage (Figure S15). Among the structural forms shown in Figure S15, **B** and **C** cannot form a quinone complex because of highly substituted salicyl rings, while **A** also cannot undergo oxidation on the account of absence of isopropyl substituents on the benzidine ring. Thus, an intricate balance of both electronic and steric effects in the ligand design (as in **D**) produces the desired result.

The mechanism of conversion of **1** to **2** was further investigated through extensive UV−vis−near infrared (NIR) studies carried out as a function of temperature and time. Because we wanted to establish the exact onset of conversion of **1** to **2** under oxygen, the reagents $CuCl_2{\cdot}2H_2O$ and ligand (H_2L^1) were mixed with MeOH at −40 °C in the sample holder of the UV−vis spectrometer and the spectrum was recorded (Figure 4a). At this temperature, there was no production of **2** as revealed by the absence of quinone absorption. This solution was allowed to warm up slowly and the spectrum was recorded at intervals of 10 °C. As it can be seen from Figure 4a, the quinone absorption at 463 nm starts to appear only near RT with the peak becoming prominent at 30 °C. This explains why the reactions carried out at RT or above only produce **2**. In a second experiment, the reagents were mixed at RT and the reaction was followed as a function of time for a period of up to 3 h at the intervals of 10 min (Figure 4b). These studies indicate that as the reaction time increases, the absorption intensity of the 463 nm peak due to the quinone moiety and the absorption due to ligand field bands at 923 and 827 nm as well increase in the vis−NIR region (Figure 4b), revealing increase in the concentration of **2** as a function of time. It has also been established that the enhancement in intensity of the bands on production of **2** corresponds to pseudo-first order kinetics (k_{obs} = 5.57 ± 0.33 × 10^{-2} h^{-1}) (Figure 4c). At the end of the UV−vis experiment, the reaction mixture obtained was subjected to gas chromatography−MS (GC−MS) analysis (Figure S18). The GC fraction obtained at a retention time of 6.9 min contained substantial amounts of salicylaldehyde (m/z 122.0) released during the conversion of **1** to **2**. The fraction with a retention time of 12.5 min contained very small amounts of decomplexed amino-quinone (m/z 367.2) along with a further oxidized bis-quinone derivative (m/z 382.3).

Having established through combined UV−vis and mass spectroscopic studies that the conversion of **1** to **2** takes place via a hydrolysis−oxidation pathway, the source of oxygen in quinone formation was investigated through labelling studies. To achieve this the green solution of **1** produced under nitrogen atmosphere was reacted with $^{18}O_2$ producing the brown compound **2**. Examination of this solution by ESI−MS studies reveal the shifting of the $[M]^+$ ion peak from m/z 1003.39 to 1011.56 (8 mass number difference) (Figure 5). Based on all these experimental observations, the mechanism

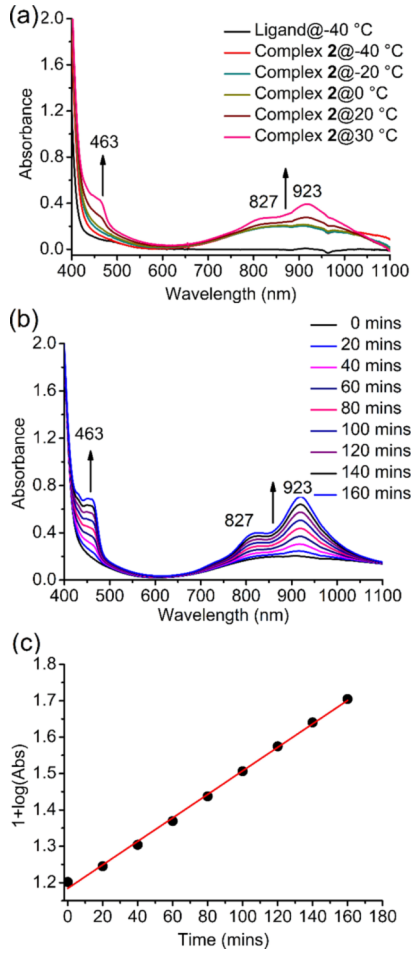

Figure 4. Progress of the reaction of in situ generated **1** (5.0 × 10^{-3} M) with O_2 in MeOH to produce **2** as a function of (a) temperature and (b) time at RT. (c) Plot of [1 + log(abs)] vs time observed at 923 nm.

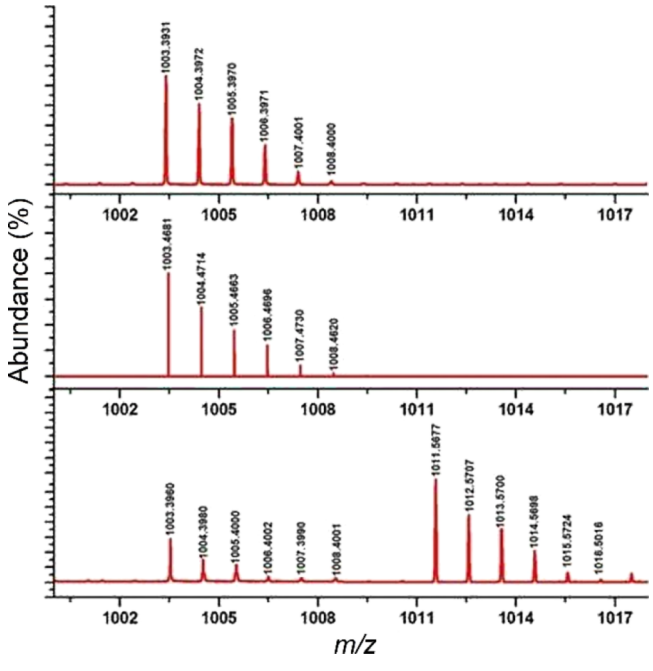

Figure 5. ESI-MS spectrum of **2** (top) and the sample prepared using $^{18}O_2$ enriched oxygen (bottom).

DOI: 10.1021/acscatal.9b02326
ACS Catal. 2019, 9, 10940−10950

shown in Figure 6 can be discerned for this unusual transformation. In the first step, dioxygen attacks the Cu(II)

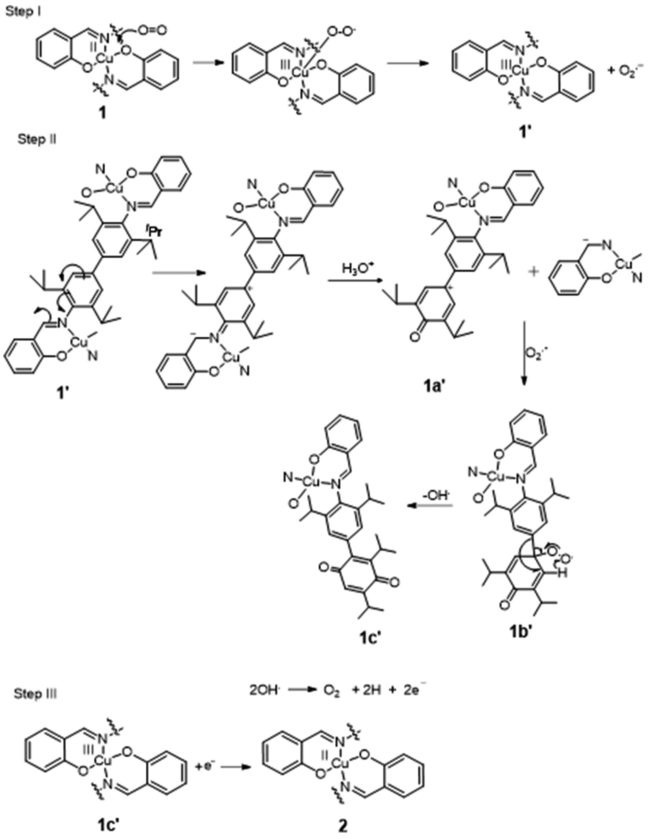

Figure 6. Proposed reaction mechanism for formation of **2** from dinuclear {Cu(III)−Cu(II)} (**1′**) species.

center of the in situ generated **1** to obtain transient Cu^{III}-superoxo species, which dissociates to a superoxide radical anion and a Cu(III) intermediate species stabilized by the strongly coordinating phenolate oxygen donor.[11]

In the second step, the positive charge on the imine nitrogen coordinated to copper(II) leads to electronic shifts followed by hydrolysis of the C═N bond to give the cationic *p*-benzoquinone intermediate. The superoxide anion radical then attacks the positive charge on this intermediate which is followed by electronic rearrangements and a 1,2-shift of the phenyl ring to generate the oxidized ligand HL^2 bound to Cu(II). When the reaction was performed in the presence of dimethyl sulfoxide (DMSO) or 3,5-di-*tert*-butyl catechol (superoxide radical scavengers),[12] no such oxidation of H_2L^1 was observed, supporting the involvement of the superoxide radical as the reactive oxygen species (also see Supporting Information, Figure S5).

Computational Studies. To gain insight into the formation of **2**, we have undertaken detailed DFT calculations.[13] The mechanism of dioxygen activation by dinuclear Cu(II) complexes has already been established.[11] Hence, we began the calculations from "step II" as depicted in Figure 6. The formation of Cu(III)-superoxide species, following the generation of the oxidized Cu(III) center and a superoxide radical, has been observed through combined electrochemical and EPR spin-trap experiments.[11,14] The mechanistic scheme adapted starting from this point is shown in Figure 6. The initial species is expected to be a mixed valent Cu(II)−Cu(III) species. The optimized structures of the computed species **1′**, **1a′**−**1c′**, and **2** along with the spin density plots are shown in Figure 7.

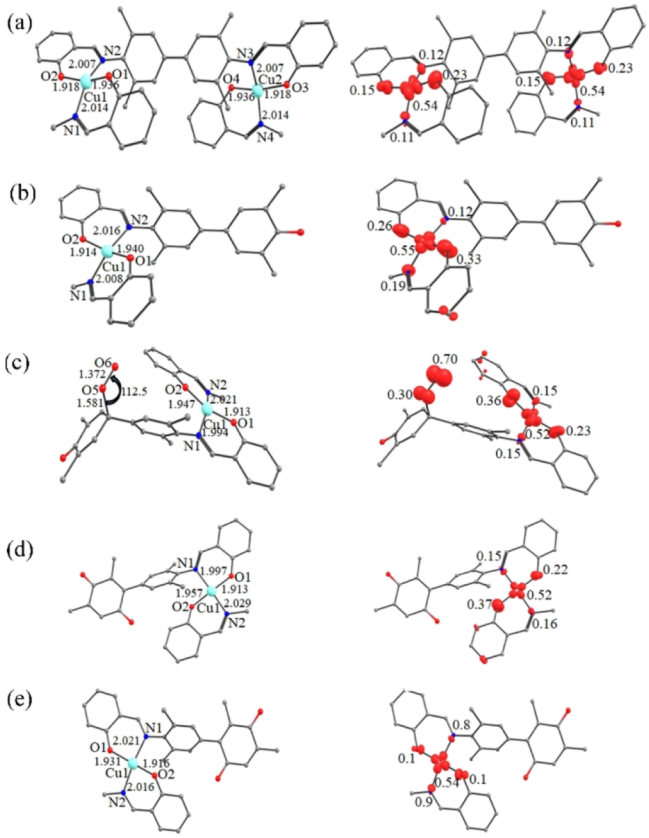

Figure 7. B3LYP-D2-optimized structures and spin density plots of (a) $^4\mathbf{1}'_{hs}$ state, (b) $^3\mathbf{1a}'_{hs}$ state, (c) $^4\mathbf{1b}'_{hs}$ state, (d) $^3\mathbf{1c}'_{hs}$, and (e) $^2\mathbf{2}_{hs}$ species, which pertains to an LMCT transition from the ligand π^* orbital to Cu(II) $d_{x^2-y^2}$ orbital (see Figure S20 in Supporting Information). Further, the computed g-tensors for species **2** (g_1 = 2.158, g_2 = 2.056 and g_3 = 2.036 for $^2\mathbf{2}_{hs}$ state) are characteristic of axial copper(II) ($g_3 > g_1 \approx g_2$) with one unpaired electron in the $d_{x^2-y^2}$ orbital (see Figure S21). These are in agreement with the observed spectral features of **2**.

Unlike the anticipated localized electronic state of [Cu(III), Cu(II)] for intermediate **1′**, the present calculations reveal a valence delocalized picture with significant spin densities on both the copper centers, as a higher symmetry is preserved with each copper ion being in an oxidation state of 2.5.

The computed energy profile for this reaction is depicted in Figure S19 (in Supporting Information). The formation of species **1b′** is estimated to be endothermic (85.1 kJ/mol at S = 1/2), suggesting that hydrolysis is a slow step. In the next step, dioxygen attack at the ipso position of the quinone moiety is expected (species **1b′**). This step is computed to be exothermic with an energy margin of −33.8 kJ/mol at S = 1/2. The computed results reveal the presence of significant spin densities both at oxygen and copper centres. Particularly, a significant spin density is detected at the distal oxygen atom, revealing the presence of oxyl radical character, which is capable of activating C−H bonds (Figure 7c). In the next step, quinone **1c′** formation is expected and one electron reduction of **1c′** leads to the formation of the final product **2**. The formation of **1c′** is exothermic (223.7 kJ/mol at S = 1/2) and

DOI: 10.1021/acscatal.9b02326
ACS Catal. 2019, 9, 10940−10950

Table 1. Products of Aerobic Oxidation of Primary Benzylic[a] and Alkyl[b] Amines Catalyzed by $[Cu(L^2)_2]$ (2)[d]

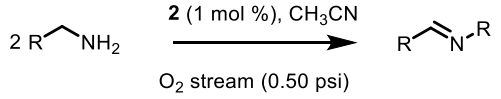

Entry	Substrate	Product	Time (h)	Temp (°C)	Yield (%)	Conversion (%)
1	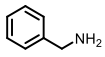	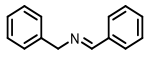	0.5	25	93	100
2	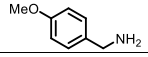	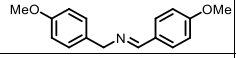	0.5	25	90	100
3	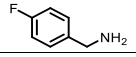	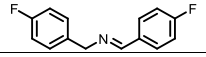	0.5	25	88	100
4	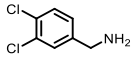	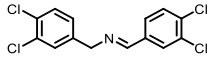	0.5	25	94	100
5	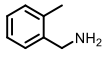	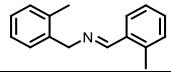	0.5	25	85	100
6	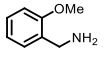	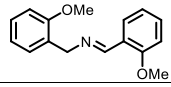	0.5	25	95	100
7	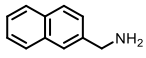	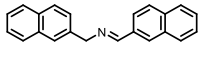	0.5	25	92	100
8	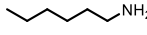	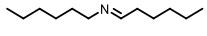	15	60	c	100
9	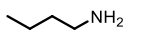	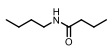	15	60	c	100

[a]Conditions: amine substrate (1.0 mmol), $[Cu(L^2)_2]$ (0.01 mmol, 1.0 mol %), O_2, CH_3CN (5 mL), RT, 30 min. [b]Conditions: amine substrate (1.0 mmol), $[Cu(L^2)_2]$ (0.01 mmol, 1.0 mol %), O_2, CH_3CN (5 mL), 60 °C, 15 h. [c]Decomposes in column. [d]By ESI−MS and ^1H NMR spectroscopy.

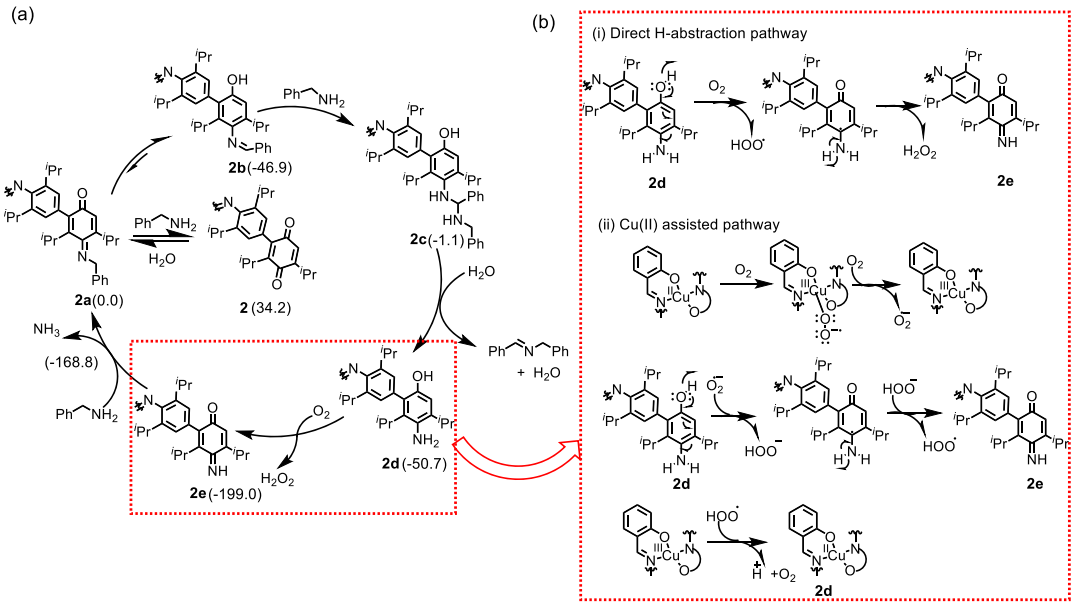

Figure 8. (a) Catalytic cycle for the production of imines from benzylic amines (energies in parenthesis, in kJ/mol). (b) Aerobic oxidation of reduced **2d** by (i) direct H-abstraction and (ii) Cu(II) assisted pathways.

hence expected to be facile. One electron reduction of **1c′** to **2** is also exothermic (536.4 kJ/mol). This suggests that once the hydrolysis takes place, all the other steps are rapid, supporting the involvement of O_2 in the generation of quinone.

Apart from computing the energetics of formation, we have also computed the spectral features of species **2** to corroborate with the experimental findings. Particularly, the computed value of ν(C═O) for complex **2** (1628 cm^{-1}) is in agreement with the experimental value (1645 cm^{-1}). Besides, time-

DOI: 10.1021/acscatal.9b02326
ACS Catal. 2019, 9, 10940−10950

dependent DFT (TDDFT) calculations reveal two intense bands at 266 and 427 nm (see Figure S20 in Supporting Information) which are in agreement with the experimental observations. The band observed at 266 nm is the MLCT band, while that at 427 nm pertains to an LMCT transition from the ligand π^* orbital to Cu(II) $d_{x^2-y^2}$ orbital.

Catalytic Amine Oxidation Reactions. Imines are valuable substrates in many organic reactions and are intermediates in the synthesis of fine chemicals.[15] They are excellent starting materials for the synthesis and racemization of chiral amines and as pharmacophores in biologically active compounds.[16] The oxidative coupling of primary amines with aldehydes and ketones to give imines can be achieved in the presence of O_2 utilizing the recently developed mild and green catalysts, but this conversion suffers from limitations such as substrate scope, enriched oxygen conditions, low turnover, use of expensive metals, tendency to decompose, longer reaction times, and need for higher reaction temperatures.[17] The fact that **2** contains two TPQ-like units prompted us to investigate its use as a catalyst for the conversion of amines to imines. Interestingly, benzylic amines when treated with 1.0% mol of **2** in CH_3CN at 25 °C in the presence of molecular oxygen completely transform to the corresponding secondary imines within 30 min, with the isolated yields ranging from 70 to 90% (Table 1; Figures S24−S39). The nonbenzylic long alkyl chain amines, however, require longer periods and higher temperatures for the completion of the reaction. In the case of the last entry, the formation of carboxylic acid results in isolation of an amide.[16,18] These results are greatly encouraging because many of the earlier organocatalytic systems containing the *p*-quinone moiety employed for the oxidation of amines to imines using dioxygen are effective only at high temperatures and/or longer reaction periods.[17e,f]

The catalytic oxidation of benzylic amines can be explained by invoking the mechanism depicted in Figure 8, which is in line with that already proposed for the CAO enzyme-based biochemical model studies.[19] The primary amine condenses with the quinone moiety of **2** to give iminoquinone **2a** (a net two electron oxidation), which tautomerizes to **2b**. Addition of a second equivalent of benzylamine yields aminal **2c** which undergoes hydrolysis to yield the product (imine) and the reduced *p*-aminohydroquinone **2d**. Aerobic oxidation of **2d** yields iminoquinone **2e**, which undergoes transamination with the substrate to give NH_3 and regenerates **2a**. The tautomeric form **2b** is stabilized by the neighboring phenyl ring. The Cu(II) in **2d** reacts with dioxygen to generate a Cu(III) intermediate and superoxide anion radical, which then abstracts hydrogen from the phenolic hydroxyl group to give HO_2^-, which combines with H^+ in solution to generate H_2O_2. This facilitates the abstraction of one of the two hydrogen atoms of the amine group by O_2 to form **2e** (Figure 8).

To obtain further insight into the nature of intermediates and to ascertain the role of copper ions and formation of radicals in the catalysis, we have added radical scavengers (DMSO or 3,5-di-*tert*-butyl catechol) in the oxidation of the 2-methoxy benzylamine substrate (entry 6 in Table 1). These experiments showed that when DMSO or catechol is used as a radical scavenger, no reaction took place (see Supporting Information Figures S42 and S43 for corresponding GC−MS traces). These experiments clearly suggest a significant contribution of the copper ion in the catalysis. The H_2O_2 formed transfers one electron to Cu(III) to regenerate the catalyst. This observation provides an indirect evidence for the role of copper in the active site of CAO in the oxidation half reaction of the enzyme.

Additionally, the cyclic voltammogram of **2** in acetonitrile is recorded at RT which shows two ligand-based redox events at lower potentials, a reversible Cu(II)/Cu(III) couple is also observed at the higher potentials (see Figure 9). These values

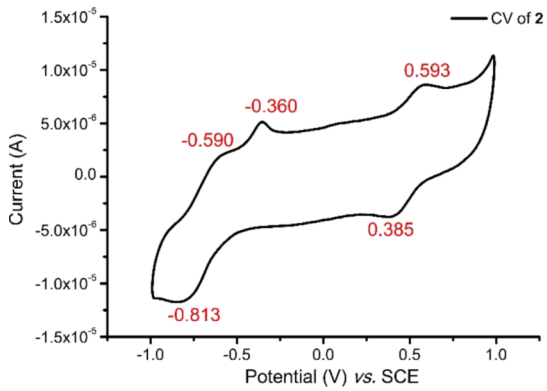

Figure 9. Cyclic voltammogram of **2** in acetonitrile showing three redox events of which the event occurring at a higher potential corresponds to the Cu(II)/Cu(III) couple (reference potential 0.242 V vs normal hydrogen electrode).

are similar to those of the earlier observed oxidation of Cu(II) to Cu(III) redox couple.[20] These data also corroborate with the DFT calculated results where the α-spin highest occupied molecular orbital which is primarily present on the metal $d_{x^2-y^2}$ orbital while the β-spin lowest unoccupied molecular orbital is completely centered on *para*-quinone (Figure S23).

This suggests that any oxidation performed on **2** is likely to yield Cu(III) species while reduction is expected to take place at the ligand center. This contrasts the earlier suggestion that copper interacts with the 4-hydroxyl group present in the TPQ cofactor to stabilize it and that the Cu(I) oxidation state is involved in the oxidative half-reaction.[21] The present system thus provides a definitive proof for the role of Cu(II) in the enzymatic process.

To understand the above catalytic mechanism, DFT studies have been performed (Figure S40). Formation of iminoquinone **2a** from **2** is slightly endothermic (34.2 kJ/mol), while subsequent tautomerization of **2a** to **2b** is exothermic by −47.0 kJ/mol because the quinone ring gains aromaticity due to tautomerization. In species **2b**, the N=C bond is strongly polarized with a large negative charge on nitrogen and a small charge on carbon, favoring additional nucleophilic attack on carbon by the incoming benzylamine leading to **2c** (thermoneutral; −1.1 kJ/mol with respect to **2**; Figure 8). Upon addition of benzyl amine, the N−C bond weakens (N3−C2 in **2c** is 1.477 Å compared to 1.28 Å in **2b**, see Figure 8). Besides, the C−N bond is even more polarized with C possessing +0.13 and nitrogen −0.7 charges, suggesting the possibility of hydrolysis by water. This step (**2c** yielding **2d**) is also exothermic by −50.7 kJ/mol. In the next step, hydrogen atom abstraction by the oxygen molecule takes place in **2d** to yield **2e**. The final step is excessively exothermic by 199 kJ/mol. These calculations establish that the formation of **2a** from **2** is slow while other steps are facile, rationalizing shorter reaction times for catalysis. Because the overall energy computed for the cycle is exothermic, this is likely to ease

DOI: 10.1021/acscatal.9b02326
ACS Catal. 2019, 9, 10940−10950

Table 2. Aerobic Cross-Coupling of Primary Amines by 2

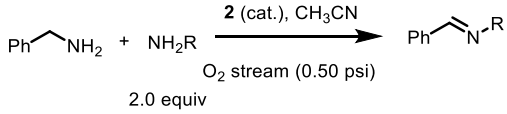

Entry	Amine	Product	Catalyst (mol %)	Time (h)	Temp^r (^{o}C)	Conversion (%)[a]	Isolated Yield (%)
1		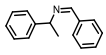	0.5	2	25	100	88
2		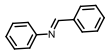	2.0	3.5	25	100	92
3		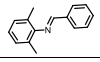	2.0	6.0	25	100	85
4		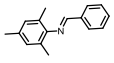	2.0	48.0	25	100	97
5		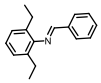	2.0	4.5	25	100	92
6		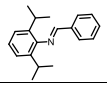	2.0	12	25	100	90
7	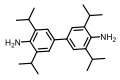	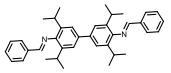	5.0	120	25	100	85

[a]By ESI−MS and ^{1}H NMR spectroscopy.

the next catalytic cycle leading to larger TON numbers as found in the experiments.

The bulky α-(+)methylbenzylamine is not oxidized under these conditions because of the methyl group at α-carbon. The catalysis is, however, observed with 2.5 mol % of **2**, yielding the imine dimer (+)-*N*-(1-phenylethyl-1-phenylethanimine) ($[\alpha]_\lambda^T$ = 91.23) after 6 h in 94% yield.

The catalyst selectivity for primary benzylic amines suggests that selective heterocoupling could be achieved by combining a benzylic amine with a less readily oxidized amine. Coupling of α-(+)methylbenzylamine with benzylamine required less catalyst loading (0.5%) than the homocoupling reactions (Table 2). Upon increasing the catalyst loading to 2 mol %, cross-coupled products were formed in good yield and desirable selectivity.

The oxidation of benzylic amines to imines were investigated with other copper complexes and salts under conditions employed above for catalyst **2**. However, no reaction was observed even after 24 h (Table S8), although it has been reported earlier that oxidation by copper salts require high temperature.[17h] Similarly, the reaction was also found not to proceed without any catalyst (blank) (Table S8, entry 1). Further, the oxidation of nonbenzylic amines with catalyst **2** did not result in any significant oxidation product even after 24 h of reaction at RT (Table S9).

CONCLUSIONS

We have demonstrated that the ligand stereo-electronic properties can be fine-tuned to successfully obtain a structural-cum-functional model for CAO enzymes. This unprecedented model contains two sterically hindered benzoquinone moieties that are analogous to the TPQ cofactor. More importantly, it acts as a robust biomimetic catalyst for the chemoselective conversion of primary amines to secondary imines under ambient conditions using environmentally benign oxidant. It appears that the copper ion in complex **2** may have a role in the catalytic conversion because other organocatalysts employed earlier for this reaction do not exhibit similar reactivity or efficiency. In this context, the role of copper ions needs to be further investigated by modifying the ligand systems.

EXPERIMENTAL SECTION

Materials and Methods. *Materials.* All the solvents were distilled and purified as described in the literature.[22] All the starting materials and the products were found to be stable toward moisture and air, and hence no specific precautions were taken in handling. Commercially available starting materials such as 2,6-diisopropylaniline (Alfa Aesar) and salicylaldehyde (Merck) were used as such. All the aliphatic amines were purchased from Spetrochem Chemicals. 4-Bromo-2,6-diisopropylaniline, 2,2′,6,6′-tetraisopropylbenzidine and Schiff-base ligands H_2L^1, H_2L^3, and H_2L^4 were synthesized according to the published procedures.[8,23]

Physical Measurements. The melting points were measured in glass capillaries and are reported uncorrected. Elemental analyses were performed on a Thermo Finnigan (FLASH EA 1112) microanalyzer. IR spectra were recorded on a PerkinElmer Spectrum One IR spectrophotometer as KBr diluted discs. NMR spectra were recorded on a Bruker Avance DPX-400 and 500 MHz spectrometers using Me_4Si as an internal reference for proton. ESI−MS was performed on a

DOI: 10.1021/acscatal.9b02326
ACS Catal. 2019, 9, 10940−10950

Bruker Maxis Impact or Waters Q-TOF micro mass spectrometer. Thermogravimetric analyses were performed on a PerkinElmer Pyris Diamond TGA instrument in the temperature range 25−1000 °C under a stream of nitrogen gas. Electronic absorption spectra were recorded on a Varian Cary Bio 100 UV−vis spectrophotometer. The temperature-dependent UV−vis spectra were recorded on an Agilent 8453 diode array-based UV−vis spectrophotometer. The EPR measurements were made with a JEOL model FA200 and a Bruker EMX plus electron spin resonance spectrometers. Cyclic voltammetry was carried out on a PAR VersaStat 4 potentiostat (Ametek) under a nitrogen atmosphere. A standard three-electrode setup was used where glassy carbon as a working electrode, platinum wire as an auxiliary electrode, and saturated calomel electrode as a reference electrode with a scan rate of 100 mV s^{-1} were used. 0.1 M tetraethylammonium perchlorate was used as the supporting electrolyte with a substrate concentration of 10^{-3} M.

X-ray Diffraction Studies. The X-ray diffraction data for **2** and **3** were collected on a Rigaku Saturn 724+ CCD diffractometer with a Mo Kα radiation source (λ = 0.71075 Å) at 150 K and a Cu Kα radiation source (λ = 1.54190 Å) at 100 K, respectively, under continuous flow of cooled nitrogen gas. The data integration and indexing were performed using Rigaku Crystal clear software and a multiscan method was employed to correct for absorption. All the calculations were carried out using the programs in the WinGX.[24] The structure solution was obtained by direct methods using SIR-92 program.[25] The final refinement of the structure was carried out using full least-square methods on F^2 using SHELX-14.[26] All nonhydrogen atoms were refined anisotropically. The hydrogen atoms were refined isotropically as rigid atoms in their idealized locations. The unassigned electron densities corresponding to the severely disordered solvent molecules in compound **3** was flattened using the SQUEEZE subroutine of PLATON.[27] The solvent accessible volume in **3** was 3123 $Å^3$ and the electrons found in S.A.V. per unit cell were 508. The X-ray structure determination details have been deposited at the CCDC with the deposition numbers 1431820 and 1836063.

*Synthesis of [Cu(L^2)$_2$] (**2**) (HL^2 = 2-(2,6-Diisopropylphenyl)-imino)methyl)phenol)-3,5-diisopropylbenzoquinone).* H_2L^1 (0.022 g, 0.04 mmol)[8] was dissolved in the dichloromethane (DCM)/MeOH mixture (5/15 mL). A methanolic solution (25 mL) of $CuCl_2·2H_2O$ (0.017 g, 0.1 mmol) was added to this solution under stirring. A green solution which appeared immediately turned brown within a few minutes. After two weeks, brown needle shaped crystals were formed on the wall of the beaker, which were suitable for single crystal X-ray diffraction studies. The crystals were washed with small amounts of cold DCM and MeOH and dried under vacuum. Yield, 60%. mp >200 °C. Anal. Calcd for $C_{62}H_{72}CuN_2O_6$: C, 74.11; H, 7.22; N, 2.79. Found: C, 73.82; H, 6.99; N, 2.84. FT-IR (KBr disc, cm^{-1}): 3427 (b), 2958 (s), 2925 (s), 2866 (s), 1645 (s), 1610 (s), 1453 (s) 1443 (s), 1320 (s), 1181 (s), 1059 (w), 872 (w), 813 (w), 696 (s). ESI−MS calcd for $C_{62}H_{72}CuN_2O_6$: 1003.4681 (100.0%), 1004.4714 (67.1%), 1005.4663 (44.6%), 1006.4696 (29.9%), 1007.4782 (22.1%), 1008.4780 (9.9%); observed: 1003.3931 (100.0%), 1004.3972 (67.1%), 1005.3971 (44.6%), 1006.3971 (29.9%), 1007.4001 (22.1%), 1008.4500 (9.9%). UV−vis (MeOH, λ_{max}, nm): 210, 265, 463.

*Synthesis of [Cu(L^4)]$_n$ (**4**).* The Schiff-base ligand H_2L^4 (0.021 g, 0.034 mmol) was taken in CH_2Cl_2 (5 mL) in a 100 mL beaker and $CuCl_2·2H_2O$ (0.015 g, 0.08 mmol) dissolved in CH_3OH (20 mL) was added to this with stirring. A brown solution was obtained immediately which was kept undisturbed on the benchtop. After 48 h brown block shaped crystals were obtained from this solution which were found to be suitable for X-ray diffraction studies. Yield: 0.010 g (42% based on H_2L^4). mp >250 °C. Anal. Calcd for **4**·MeOH ($C_{43}H_{54}CuN_2O_3$): C, 72.70; H, 7.66; N, 3.94. Found: C, 71.70; H, 7.46; N, 3.99. FT-IR (KBr, cm^{-1}): 2963 (s), 2925 (s), 2871 (s), 1624 (s), 1597 (s), 1549 (s), 1463 (s), 1427 (s), 1410 (s), 1388 (s), 1320 (s), 1250 (s), 1171 (s), 1048 (s), 824 (w). EPR (polycrystalline): g_1, 2.247; g_2, 2.161; g_3, 2.044 at RT; g_1, 2.248; g_2, 2.171; g_3, 2.044 at 77 K; EPR (toluene, 100 K): $g_{\|}$, 2.210; $A_{\|}$, 179 × 10^{-4} cm^{-1}.

Reaction of $CuCl_2·2H_2O$ with H_2L^3. Reaction with bis(*N*-salicylidene-4,4-diphenylamine) (H_2L^3) to give **3**:[23a] H_2L^3 (0.025 g, 0.06 mmol) was dissolved in hot DCM (20 mL). To this solution, $CuCl_2·2H_2O$ (0.027 g, 0.15 mmol) in MeOH (25 mL) was added with stirring. The green solution that appeared, was analyzed by ESI−MS. ESI−MS for $C_{26}H_{22}Cl_2Cu_2N_2O_4$ (*m*/*z*): $[M + K]^+$ = 663.56, correspond to $[Cu(L^3)]_n$.

*Oxygenation Studies of [CuL^1]$_n$ (**1**).* The oxygenation reaction of $[CuL^1]_n$ to give **2** was examined by exposing a solution of the former complex generated in situ in methanol to molecular oxygen. Kinetic analysis of the oxygenation reaction was carried out by time-dependent measurements of the disappearance of the ligand band around 381 nm or the growth of the 923 nm ligand field band.

Labeling Studies Using $^{18}O_2$. Oxygenation reaction of a green solution of $[CuL^1]_n$ to give **2** was carried out in an inert atmosphere by exposing the solution to $^{18}O_2$ for a few minutes to yield 18-O labelled **2**. This product was examined by ESI−MS for the incorporation of the labeled oxygen producing the M^+ ion peak at 1011.5677 instead of 1003.3960.

Typical Procedure for Oxidation of Benzylamine and Its Derivatives. Benzylamine (1.0 mmol) was taken in a 25 mL two necked round bottom flask. When a solution of **2** (10 mg, 0.01 mmol) in anhydrous MeCN (5 mL) was added to it, a green solution was obtained immediately. O_2 (0.50 psi) was bubbled continuously through this solution and the reaction was stirred at RT for 30 min upon which the green solution turned into red. The reaction was monitored by ESI−MS and thin-layer chromatography (TLC). The reaction mixture was then concentrated by rotary evaporation and conversion % was analyzed by ^{1}H NMR. The product was purified by using a column containing Et_3N-washed silica gel using pet-ether and ethyl acetate in 10:1 ratio.

Typical Procedure for n-Hexylamine and n-Butylamine Oxidation. The *n*-alkylamine (1.0 mmol) was taken in a 25 mL two-necked round bottom flask. A solution of 2 (10 mg, 0.01 mmol) in anhydrous MeCN (5 mL) was added to it, immediately a green solution was obtained. O_2 (0.50 psi) was then bubbled continuously through this solution and the reaction was stirred at RT for 2 h and then heated at 60 °C for 15 h, during which the green solution turned red. The reaction was monitored by ESI−MS and TLC. The reaction mixture was then concentrated by rotary evaporation and conversion % was analyzed by ^{1}H NMR.

Procedure for the Oxidation of Methylbenzylamine to N-(1-Phenylethyl-1-phenylethanimine). Methylbenzylamine

DOI: 10.1021/acscatal.9b02326
ACS Catal. 2019, 9, 10940−10950

(130 μL, 1.0 mmol) was taken in a 25 mL two-necked round bottom flask. When a solution of **2** (25 mg, 0.025 mmol) in anhydrous MeCN (5 mL) was added to it, a green solution was obtained immediately. O_2 (0.50 psi) was bubbled continuously through this solution and the reaction was stirred at RT for 6 h upon which the green solution turned into red. The reaction was monitored by ESI−MS and TLC. The reaction mixture was then concentrated by rotary evaporation and conversion % was analyzed by ^{1}H NMR. The product was purified by using a column containing Et_3N-washed silica gel using pet-ether and ethyl acetate in 10:1 ratio.

Typical Procedure for the Oxidation of Cross-Coupled Amines. Benzylamine (110 μL, 1.0 mmol) and methylbenzylamine or aniline (2.0 mmol) were taken in a 25 mL two-necked round bottom flask. When a solution of **2** (0.005−0.05 mmol) in anhydrous MeCN (5 mL) was added to it, a green solution was obtained immediately. O_2 (0.50 psi) was bubbled continuously through this solution and the reaction was stirred at RT for 2−120 h upon which the green solution turned into red. The reaction was monitored by ESI−MS and TLC. The reaction mixture was then concentrated by rotary evaporation and conversion % was analyzed by ^{1}H NMR. The product was purified by using a column containing Et_3N-washed silica gel using pet-ether and ethyl acetate in 10:1 ratio.

Decomplexation of 2. Method A: complex **2** (0.020 g, 0.02 mmol) was dissolved in a mixture of MeOH (30 mL) and CH_3CN (20 mL) and stirred for a while. Dry HCl gas (generated from NaCl and conc. H_2SO_4) was bubbled into this solution for an hour. During this period the brown solution turned yellow. ESI−MS for $C_{24}H_{33}NO_2$ (m/z): $[M + H]^+$ 367.53, for $C_{31}H_{37}NO_3$ (m/z): $[M + H]^+$ 471.28. Method B: to the methanolic solution (5 mL) of complex **2** (0.020 g, 0.02 mmol) was added conc. HCl (2 mL). The brown solution turned to yellow immediately. The solution was kept undisturbed and an orange precipitate was obtained after 5 days. GC−MS for $C_{24}H_{35}NO_2$ (m/z): 369.4.

Computational Details. All the calculations have been performed using the Gaussian 09 suite.[13a] The UV−vis spectral parameter of the species were computed using ORCA 2.9 software suite incorporating COSMO solvation effects.[28] The geometries were optimized using the B3LYP-D2 functional, incorporating the dispersion correction proposed by Grimme et al.[29] We have used to two different basis sets; LanL2DZ, which encompasses a double-ζ quality basis set with the Los Alamos effective core potential for Cu and a 6-31G basis set for the other atoms (C, O, N, and H).[30] A single point calculation was performed using the TZVP basis set for all the atoms.[31] An additional set of calculations performed with all the electron basis sets on Cu, does not improve the energies computed, these results are given in Supporting Information (see Figure S48). Frequency calculation on the optimized structures were undertaken to confirm the minima on the potential-energy surface and also to obtain zero-point energy corrections. The quoted DFT energies are B3LYP-D2 solvation energy including free-energy corrections from the frequency calculations at a temperature of 298.15 K. The role of solvation on the structures and energetics was studied at the B3LYP-D2 level using the polarizable continuum solvent model using methanol as the solvent.[32] All spectroscopic parameter calculations incorporate relativistic effect via the zeroth-order regular approximation method as implemented in the ORCA suite.[33] Calculation of *g*-anisotropy incorporates spin−orbit coupling using mean-field approximation and this methodology has been widely employed to compute the *g*-anisotropy.[14] TD-DFT implemented in the ORCA program was used for the calculation of excitation energies. MO visualizations were done using Chemcraft software.[34]

■ ASSOCIATED CONTENT

Supporting Information

The Supporting Information is available free of charge on the ACS Publications website at DOI: 10.1021/acscatal.9b02326.

Additional figures, crystallographic details, and spectral characterization (PDF)

Crystallographic information of **2** and **4**. CCDC 1431820 (**2**) and 1836063 (**4**) contain the supplementary crystallographic data for this paper. These data can be obtained free of charge from The Cambridge Crystallographic Data Centre (CIF)

■ AUTHOR INFORMATION

Corresponding Authors

*E-mail: rajaraman@chem.iitb.ac.in (G.R.).
*E-mail: palaniandavarm@gmail.com (M.P.).
*E-mail: rmv@chem.iitb.ac.in (R.M.).

ORCID

Gopalan Rajaraman: 0000-0001-6133-3026
Ramaswamy Murugavel: 0000-0002-1816-3225

Present Address

†Bharathidasan University, Tiruchirappalli-620024, India.

Author Contributions

R.J., M.A., and D.K. contributed equally to various aspects of this work.

Notes

The authors declare no competing financial interest.

■ ACKNOWLEDGMENTS

This work was supported by SERB (SB/S2/JCB-85/2014), New Delhi through a J. C. Bose Fellowship. G.R. thanks the Science and Engineering Research Board (CRG/2018/000430) New Delhi, for financial support. The authors thank the IITB multifrequency EPR facility for EPR measurements. The authors thank R. Marimuthu for his help in EPR studies and Professor G. K. Lahiri for providing valuable insights into the EPR studies during the revision of the manuscript. Dedicated to Professor M. S. Balakrishna on the occasion of his 60th birthday.

■ REFERENCES

(1) Largeron, M.; Fleury, M.-B. Bioinspired oxidation catalysts. *Science* **2013**, *339*, 43−44.

(2) Que, L.; Tolman, W. B. Biologically inspired oxidation catalysis. *Nature* **2008**, *455*, 333−340.

(3) (a) Eckert, T. S.; Bruice, T. C. Chemical properties of phenanthrolinequinones and the mechanism of amine oxidation by o-quinones of medium redox potentials. *J. Am. Chem. Soc.* **1983**, *105*, 4431−4441. (b) Wendlandt, A. E.; Stahl, S. S. Chemoselective organocatalytic aerobic oxidation of primary amines to secondary imines. *Org. Lett.* **2012**, *14*, 2850−2853. (c) Leon, M. A.; Liu, X.; Phan, J. H.; Clift, M. D. Amine Functionalization through Sequential Quinone-Catalyzed Oxidation/Nucleophilic Addition. *Eur. J. Org. Chem.* **2016**, 4508−4515.

(4) Yuan, H.; Yoo, W.-J.; Miyamura, H.; Kobayashi, S. Discovery of a metalloenzyme-like cooperative catalytic system of metal nano-

DOI: 10.1021/acscatal.9b02326
ACS Catal. 2019, 9, 10940−10950

clusters and catechol derivatives for the aerobic oxidation of amines. *J. Am. Chem. Soc.* **2012**, *134*, 13970−13973.
(5) (a) Largeron, M.; Fleury, M.-B. A Biologically Inspired CuI/Topaquinone-Like Co-Catalytic System for the Highly Atom-Economical Aerobic Oxidation of Primary Amines to Imines. *Angew. Chem., Int. Ed.* **2012**, *51*, 5409−5412. (b) Largeron, M.; Fleury, M.-B. A Metalloenzyme-Like Catalytic System for the Chemoselective Oxidative Cross-Coupling of Primary Amines to Imines under Ambient Conditions. *Chem. - Eur. J.* **2015**, *21*, 3815−3820.
(6) (a) Murray, J. M.; Saysell, C. G.; Wilmot, C. M.; Tambyrajah, W. S.; Jaeger, J.; Knowles, P. F.; Phillips, S. E. V.; McPherson, M. J. The Active Site Base Controls Cofactor Reactivity inEscherichia coli Amine Oxidase: X-ray Crystallographic Studies with Mutational Variants. *Biochemistry* **1999**, *38*, 8217−8227. (b) Wilmot, C. M.; Murray, J. M.; Alton, G.; Parsons, M. R.; Convery, M. A.; Blakeley, V.; Corner, A. S.; Palcic, M. M.; Knowles, P. F.; McPherson, M. J.; Phillips, S. E. V. Catalytic Mechanism of the Quinoenzyme Amine Oxidase from *Escherichia coli*: Exploring the Reductive Half-Reaction. *Biochemistry* **1997**, *36*, 1608−1620. (c) Hartmann, C.; Klinman, J. P. Structure-function studies of substrate oxidation by bovine serum amine oxidase: relationship to cofactor structure and mechanism. *Biochemistry* **1991**, *30*, 4605−4611.
(7) (a) Bacon, J.; Adams, R. N. Anodic oxidations of aromatic amines. III. Substituted anilines in aqueous media. *J. Am. Chem. Soc.* **1968**, *90*, 6596−6599. (b) Rao, A. V. R.; Chavan, S. P.; Sivadasan, L. Synthesis of lavendamycin. *Tetrahedron* **1986**, *42*, 5065−5071.
(8) Jangir, R.; Kaleeswaran, D.; Murugavel, R. 2,2′,6,6′-Tetraisopropylbenzidine-Based Sterically Encumbered Ditopic C2-Symmetric Ligand Systems and Supramolecular Building Blocks. *ChemistrySelect* **2018**, *3*, 8082−8094.
(9) Haynes, R. K.; Hewgill, F. R. Amine oxidation and the chemistry of quinone imines. Part II. 2,5-Di-methoxy-4-*t*-butylaniline. *J. Chem. Soc., Perkin Trans. 1* **1972**, 408−413.
(10) (a) Chaudhuri, P.; Verani, C. N.; Bill, E.; Bothe, E.; Weyhermüller, T.; Wieghardt, K. Electronic Structure of Bis(o-iminobenzosemiquinonato)metal Complexes (Cu, Ni, Pd). The Art of Establishing Physical Oxidation States in Transition-Metal Complexes Containing Radical Ligands. *J. Am. Chem. Soc.* **2001**, *123*, 2213−2223. (b) Vaidyanathan, M.; Viswanathan, R.; Palaniandavar, M.; Balasubramanian, T.; Prabhaharan, P.; Muthiah, P. Copper(II) Complexes with Unusual Axial Phenolate Coordination as Structural Models for the Active Site in Galactose Oxidase: X-ray Crystal Structures and Spectral and Redox Properties of [Cu(bpnp)-X] Complexes. *Inorg. Chem.* **1998**, *37*, 6418−6427. (c) Mustieles Marín, I.; Cheisson, T.; Singh-Chauhan, R.; Herrero, C.; Cordier, M.; Clavaguera, C.; Nocton, G.; Auffrant, A. Electronic Structures of Mono-Oxidized Copper and Nickel Phosphasalen Complexes. *Chem.—Eur. J.* **2017**, *23*, 17940−17953. (d) Fernández-G, J. M.; Ausbun-Valdés, C.; González-Guerrero, E. E.; Toscano, R. A. Characterization and Crystal Structure of some Schiff Base Copper-(II) Complexes derived from Enantiomeric Pairs of Chiral Amines. *Z. Anorg. Allg. Chem.* **2007**, *633*, 1251−1256.
(11) Lamour, E.; Routier, S.; Bernier, J.-L.; Catteau, J.-P.; Bailly, C.; Vezin, H. Oxidation of CuIIto CuIII, Free Radical Production, and DNA Cleavage by Hydroxy-salen−Copper Complexes. Isomeric Effects Studied by ESR and Electrochemistry. *J. Am. Chem. Soc.* **1999**, *121*, 1862−1869.
(12) Beckman, J. S.; Beckman, T. W.; Chen, J.; Marshall, P. A.; Freeman, B. A. Apparent hydroxyl radical production by peroxynitrite: implications for endothelial injury from nitric oxide and superoxide. *Proc. Natl. Acad. Sci. U.S.A.* **1990**, *87*, 1620−1624.
(13) (a) Frisch, M.; Trucks, G.; Schlegel, H. B.; Scuseria, G.; Robb, M.; Cheeseman, J.; Scalmani, G.; Barone, V.; Mennucci, B.; Petersson, G. *Gaussian 09*, Revision a.02; Gaussian Inc.: Wallingford, CT, 2009; p 200. (b) Neese, F. The ORCA program system. *Wiley Interdiscip. Rev.: Comput. Mol. Sci.* **2012**, *2*, 73−78.
(14) Rajaraman, G.; Ruiz, E.; Cano, J.; Alvarez, S. Theoretical determination of the exchange coupling constants of a single-molecule magnet Fe10 complex. *Chem. Phys. Lett.* **2005**, *415*, 6−9.
(15) (a) Kobayashi, S.; Mori, Y.; Fossey, J. S.; Salter, M. M. Catalytic Enantioselective Formation of C−C Bonds by Addition to Imines and Hydrazones: A Ten-Year Update. *Chem. Rev.* **2011**, *111*, 2626−2704. (b) Largeron, M. Aerobic catalytic systems inspired by copper amine oxidases: recent developments and synthetic applications. *Org. Biomol. Chem.* **2017**, *15*, 4722−4730.
(16) Török, B.; Surya Prakash, G. K. Synthesis of Chiral Trifluoromethylated Amines by Palladium-Catalyzed Diastereoselective Hydrogenation-Hydrogenolysis Approach. *Adv. Synth. Catal.* **2003**, *345*, 165−168.
(17) (a) Liu, L.; Zhang, S.; Fu, X.; Yan, C.-H. Metal-free aerobic oxidative coupling of amines to imines. *Chem. Commun.* **2011**, *47*, 10148−10150. (b) Choi, H.; Doyle, M. P. Oxidation of secondary amines catalyzed by dirhodium caprolactamate. *Chem. Commun.* **2007**, 745−747. (c) Él, A. H.; Samec, J. S. M.; Brasse, C.; Bäckvall, J.-E. Dehydrogenation of aromatic amines to imines via ruthenium-catalyzed hydrogen transfer. *Chem. Commun.* **2002**, 1144−1145. (d) Jiang, G.; Chen, J.; Huang, J.-S.; Che, C.-M. Highly efficient oxidation of amines to imines by singlet oxygen and its application in ugi-type reactions. *Org. Lett.* **2009**, *11*, 4568−4571. (e) Kodama, S.; Yoshida, J.; Nomoto, A.; Ueta, Y.; Yano, S.; Ueshima, M.; Ogawa, A. Direct conversion of benzylamines to imines via atmospheric oxidation in the presence of $VO(Hhpic)_2$ catalyst. *Tetrahedron Lett.* **2010**, *51*, 2450−2452. (f) Lang, X.; Ji, H.; Chen, C.; Ma, W.; Zhao, J. Selective formation of imines by aerobic photocatalytic oxidation of amines on TiO_2. *Angew. Chem., Int. Ed.* **2011**, *50*, 3934−3937. (g) Nishinaga, A.; Yamazaki, S.; Matsuura, T. Catalytic dehydrogenation of secondary amines with cobalt schiff base complex-oxygen system. *Tetrahedron Lett.* **1988**, *29*, 4115−4118. (h) Patil, R. D.; Adimurthy, S. Copper-catalyzed aerobic oxidation of amines to imines under neat conditions with low catalyst loading. *Adv. Synth. Catal.* **2011**, *353*, 1695−1700. (i) Prades, A.; Peris, E.; Albrecht, M. Oxidations and Oxidative Couplings Catalyzed by Triazolylidene Ruthenium Complexes. *Organometallics* **2011**, *30*, 1162−1167. (j) So, M.-H.; Liu, Y.; Ho, C.-M.; Che, C.-M. Graphite-Supported Gold Nanoparticles as Efficient Catalyst for Aerobic Oxidation of Benzylic Amines to Imines andN-Substituted 1,2,3,4-Tetrahydroisoquinolines to Amides: Synthetic Applications and Mechanistic Study. *Chem.—Asian J.* **2009**, *4*, 1551−1561. (k) Wang, J.-R.; Fu, Y.; Zhang, B.-B.; Cui, X.; Liu, L.; Guo, Q.-X. Palladium-catalyzed aerobic oxidation of amines. *Tetrahedron Lett.* **2006**, *47*, 8293−8297. (l) Aschwanden, L.; Mallat, T.; Krumeich, F.; Baiker, A. A simple preparation of an efficient heterogeneous gold catalyst for aerobic amine oxidation. *J. Mol. Catal. A: Chem.* **2009**, *309*, 57−62. (m) Neumann, R.; Levin, M. Selective aerobic oxidative dehydrogenation of alcohols and amines catalyzed by a supported molybdenum-vanadium heteropolyanion salt Na5PMo2V2O40. *J. Org. Chem.* **1991**, *56*, 5707−5710. (n) Samec, J. S. M.; Él, A. H.; Bäckvall, J.-E. Efficient Ruthenium-Catalyzed Aerobic Oxidation of Amines by Using a Biomimetic Coupled Catalytic System. *Chem.—Eur. J.* **2005**, *11*, 2327−2334. (o) Hu, Z.; Kerton, F. M. Simple copper/TEMPO catalyzed aerobic dehydrogenation of benzylic amines and anilines. *Org. Biomol. Chem.* **2012**, *10*, 1618−1624.
(18) Giust, S.; La Sorella, G.; Sperni, L.; Strukul, G.; Scarso, A. Substrate selective amide coupling driven by encapsulation of a coupling agent within a self-assembled hexameric capsule. *Chem. Commun.* **2015**, *51*, 1658−1661.
(19) Mure, M.; Mills, S. A.; Klinman, J. P. Catalytic Mechanism of the Topa Quinone Containing Copper Amine Oxidases. *Biochemistry* **2002**, *41*, 9269−9278.
(20) (a) Ourari, A.; Aggoun, D.; Ouahab, L. A novel copper(II)−Schiff base complex containing pyrrole ring: Synthesis, characterization and its modified electrodes applied in oxidation of aliphatic alcohols. *Inorg. Chem. Commun.* **2013**, *33*, 118−124. (b) Naskar, S.; Naskar, S.; Mayer-Figge, H.; Sheldrick, W. S.; Chattopadhyay, S. K. Synthesis, X-ray crystal structures, spectroscopic and cyclic voltam-

DOI: 10.1021/acscatal.9b02326
ACS Catal. 2019, 9, 10940−10950

metric studies of Cu(II) Schiff base complexes of pyridoxal. *Polyhedron* **2011**, *30*, 529−534. (c) Amer, A. A.; Ilikti, H.; Beyens, C.; Lyskawa, J.; Maschke, U. Elaboration of new modified electrodes (MEs) by electropolymerization of Cu (II)-Schiff base complexes bearing pyrrole moieties: Application in electroreduction of acetophenone and carbon dioxide. *Eur. Polym. J.* **2019**, *112*, 569−580. (d) Dadamos, T. R. L.; Teixeira, M. F. S. Electrochemical sensor for sulfite determination based on a nanostructured copper-salen film modified electrode. *Electrochim. Acta* **2009**, *54*, 4552−4558. (e) Karaoğlu, K.; Serbest, K.; Emirik, M.; Şahin, E. An unsymmetrical ferrocene based azine and its Cu (II) complex: Spectroscopy, crystal structure, electrochemistry and DFT calculations. *J. Organomet. Chem.* **2015**, *775*, 80−87. (f) Chiang, L.; Herasymchuk, K.; Thomas, F.; Storr, T. Influence of electron-withdrawing substituents on the electronic structure of oxidized Ni and Cu salen complexes. *Inorg. Chem.* **2015**, *54*, 5970−5980. (g) Storr, T.; Verma, P.; Pratt, R. C.; Wasinger, E. C.; Shimazaki, Y.; Stack, T. D. P. Defining the Electronic and Geometric Structure of One-Electron Oxidized Copper−Bis-phenoxide Complexes. *J. Am. Chem. Soc.* **2008**, *130*, 15448−15459.

(21) Murakawa, T.; Hamaguchi, A.; Nakanishi, S.; Kataoka, M.; Nakai, T.; Kawano, Y.; Yamaguchi, H.; Hayashi, H.; Tanizawa, K.; Okajima, T. Probing the Catalytic Mechanism of Copper Amine Oxidase from *Arthrobacter globiformis* with Halide Ions. *J. Biol. Chem.* **2015**, *290*, 23094−23109.

(22) Armarego, W. L.; Chai, C. L. L. *Purification of Laboratory Chemicals*; Butterworth-Heinemann, 2013.

(23) (a) Dong, G.; Chun-qi, Q.; Chun-ying, D.; Ke-liang, P.; Qing-jin, M. Synthesis and Structural Characterization of a Novel Mixed-Valent CuIICuICuII Triangular Metallomacrocycle Using an Imine-Based Rigid Ligand. *Inorg. Chem.* **2003**, *42*, 2024−2030. (b) Wehrmann, P.; Mecking, S. Highly Active Binuclear Neutral Nickel(II) Catalysts Affording High Molecular Weight Polyethylene. *Organometallics* **2008**, *27*, 1399−1408. (c) Bhunora, S.; Mugo, J.; Bhaw-Luximon, A.; Mapolie, S.; Van Wyk, J.; Darkwa, J.; Nordlander, E. The use of Cu and Zn salicylaldimine complexes as catalyst precursors in ring opening polymerization of lactides: ligand effects on polymer characteristics. *Appl. Organomet. Chem.* **2011**, *25*, 133−145.

(24) Farrugia, L. J. WinGX suite for small-molecule single-crystal crystallography. *J. Appl. Crystallogr.* **1999**, *32*, 837−838.

(25) Altomare, A.; Cascarano, G.; Giacovazzo, C.; Guagliardi, A. Completion and refinement of crystal structures with SIR92. *J. Appl. Crystallogr.* **1993**, *26*, 343−350.

(26) Sheldrick, G. M. Crystal structure refinement with SHELXL. *Acta Crystallogr., Sect. C: Struct. Chem.* **2015**, *71*, 3−8.

(27) Spek, A. L. PLATON SQUEEZE: a tool for the calculation of the disordered solvent contribution to the calculated structure factors. *Acta Crystallogr., Sect. C: Struct. Chem.* **2015**, *71*, 9−18.

(28) Neese, F. The ORCA program system. *Wiley Interdiscip. Rev.: Comput. Mol. Sci.* **2012**, *2*, 73−78.

(29) Grimme, S. Semiempirical GGA-type density functional constructed with a long-range dispersion correction. *J. Comput. Chem.* **2006**, *27*, 1787−1799.

(30) (a) Ditchfield, R.; Hehre, W. J.; Pople, J. A. Self-consistent molecular-orbital methods. IX. An extended Gaussian-type basis for molecular-orbital studies of organic molecules. *J. Chem. Phys.* **1971**, *54*, 724−728. (b) Hay, P. J.; Wadt, W. R. Ab initio effective core potentials for molecular calculations. Potentials for K to Au including the outermost core orbitals. *J. Chem. Phys.* **1985**, *82*, 299−310.

(31) (a) Schäfer, A.; Horn, H.; Ahlrichs, R. Fully optimized contracted Gaussian basis sets for atoms Li to Kr. *J. Chem. Phys.* **1992**, *97*, 2571−2577. (b) Groves, J. T.; Gross, Z.; Stern, M. K. Preparation and Reactivity of Oxoiron(IV) Porphyrins. *Inorg. Chem.* **1994**, *33*, 5065−5072.

(32) Mennucci, B. Polarizable continuum model. *Wiley Interdiscip. Rev.: Comput. Mol. Sci.* **2012**, *2*, 386−404.

(33) (a) Römelt, M.; Ye, S.; Neese, F. Calibration of modern density functional theory methods for the prediction of 57Fe Mössbauer isomer shifts: meta-GGA and double-hybrid functionals. *Inorg. Chem.* **2009**, *48*, 784. (b) Radoul, M.; Sundararajan, M.; Potapov, A.; Riplinger, C.; Neese, F.; Goldfarb, D. Revisiting the nitrosyl complex of myoglobin by high-field pulse EPR spectroscopy and quantum mechanical calculations. *Phys. Chem. Chem. Phys.* **2010**, *12*, 7276−7289.

(34) Zhurko, G. *ChemCraft Software*, version 1.6, 2014.

DOI: 10.1021/acscatal.9b02326
ACS Catal. 2019, 9, 10940−10950